TEMPERATURE DEPENDENCE OF ESR IN CdS(I)

by

RONALD GORDON PERKIN

A THESIS SUBMITTED IN PARTIAL FULFILMENT
OF THE REQUIREMENTS FOR THE DEGREE OF
MASTER OF SCIENCE

in the Department

of

Physics

We accept this thesis as conforming to the

required standard

THE UNIVERSITY OF BRITISH COLUMBIA

In presenting this thesis in partial fulfilment of the requirements for an advanced degree at the University of British Columbia, I agree that the Library shall make it freely available for reference and study. I further agree that permission for extensive copying of this thesis for scholarly purposes may be granted by the Head of my Department or by his representatives. It is understood that copying or publication of this thesis for financial gain shall not be allowed without my written permission.

Department of Physics

The University of British Columbia
Vancouver 8, Canada

Date July 10, 1970

ABSTRACT

Previous measurements on CdS (I) have shown a temperature shift in the single electron spin resonance (ESR) impurity band line. At 34 GHz this shift was found to be:

$$\frac{dg}{dT} = -2.5 \times 10^{-4}/^{\circ}K$$

in going from $4.2^{\circ}K$ to $1.7^{\circ}K$.

This thesis presents the construction and testing of a metal temperature controlled dewar for the purpose of measuring the shift over the temperature range from $40^{\circ}K$ to $1.7^{\circ}K$ using an X-band (9 GHz) spectrometer. The signal was observed between $1.7^{\circ}K$ and $4.2^{\circ}K$ but rapidly broadened and could not be seen at higher temperatures. Since the lowest attainable temperature of the metal dewar was around $5^{\circ}K$, it could not be used as planned. Further studies using glass dewars proved that the g-shift at 9 GHz was too small to be measured.

The theory for the g-shift is discussed and the performance of the dewar evaluated.

TABLE OF CONTENTS

LIST OF FIGURES AND TABLES

ACKNOWLEDGMENTS

I would like to thank the many people who assisted in the completion of this work; particularly Dr. C. Schwerdtfeger for his help in all phases, Mr. W. Morrison for building the metal dewar, Robin Halliwell for his help in testing the dewar.

I would also like to thank Dr. C. Schwerdtfeger and Mrs. Helen Atkins for their patient assistance in the writing and typing of this thesis.

CHAPTER 1

INTRODUCTION

Earlier experiments by B. J. Slagsvold[1] exhibited a temperature dependence of the single resonance line of the impurity band in iodine doped cadmium sulphide. This effect was observed in the temperature range of from 1.7°K to 4.2°K using an electron spin resonance (ESR) spectrometer operating at a frequency of approximately 31 GHz (K_a-band). The purpose of this thesis is to further study this effect using an X-band (10 GHz) spectrometer incorporating a temperature controlled dewar designed to operate up to a temperature of 40°K and down to a temperature of 4.2°K. The construction and testing of this dewar are described, and further suggestions are made to improve its low temperature performance.

At the lowest stable temperature attainable in the dewar, 12°K, the cadmium sulphide line was too broad to be observed, therefore the dewar could not be used for this purpose. However, the temperature shift was studied at X-band frequencies in the range from 1.7°K to 4.2°K in a glass dewar system similar to the one used with the K_a-band spectrometer. The results of these experiments which were obtained from experiments using a number of highly doped Cds(I)

samples, showed no measurable temperature shift.

In going from K_a-band to X-band, one goes to a magnetic field approximately one third as great. Because of this, the error in field measurement must also be one third as great in order to maintain the same per cent accuracy. Therefore, since the expected temperature shift was in the fifth figure of the g-value, this field measurement was extremely critical. Experiments using a marginal oscillator type of nuclear magnetic resonance (NMR) probe with a glycerin sample achieved only borderline accuracy. However, sufficient accuracy was obtained using a commercial NMR probe so that a definite statement about the temperature shift could be made. Further attempts were made to observe the shift in the K_a-band spectrometer and these efforts are being continued.

CHAPTER 2

THEORY OF THE ELECTRON SPIN RESONANCE SIGNAL

Electron spin resonance (ESR) involves the resonant absorption of r.f. radiation by unpaired electrons in a magnetic field. For a free electron, $S=\frac{1}{2}$, there are two energy levels in a magnetic field given by

$$E = g\mu H m_J \; ; \quad m_J = \pm \tfrac{1}{2}$$

where μ is the Bohr magneton, H the magnetic field, m_J the projection of S on the direction of the magnetic field and g the spectroscopic splitting factor. ($g= 2.0023$ for a free electron.)

Since one doesn't observe free electrons but rather electrons in crystals or free radicals the g-value deviates from the above value. The major factors affecting the g-value are spin-orbit interaction, crystalline field environment and interaction with other spins both electronic and nuclear.

One of the chief sources of unpaired electrons in semiconductors is from impurities which act as donors. In the present investigation chlorine is introduced into the CdS lattice. The chlorine substitutes for the sulfur leaving one unpaired electron.

When such an ion is placed into a semiconductor two basic models can be used to describe the situation occurring:

1 The localized electron model - here the unpaired electron is localized near the lattice site occupied by the impurity ion. This is the crystal field approach developed by Abragam and Pryce in which they write a so-called "spin Hamiltonian" of effective spin S' (i.e. they observe (2S'+ 1) lines in the ESR spectrum). This is a polynomial in S' which is essentially the free ion Hamiltonian augmented with energy terms associated with the presence of the host lattice.

2 Non-localized electron model - here the unpaired electrons are so non-localized, i.e. they move easily through the crystal, that their resonance properties are determined largely by the energy band structure of the host lattice.

This investigation is concerned mainly with the second model for which the g-values are given by: (1)

$$g_{\parallel} = 2 + \lambda \frac{4}{m} \sum_{m}{}' \frac{\langle o\uparrow|p_x|m\rangle\langle m|p_y|o\uparrow\rangle}{E_o - E_m}$$

$$g_{\perp} = 2 - \lambda \frac{2}{m} \sum_{m}{}' \frac{1}{E_o - E_m} \left\{\langle o\uparrow|p_x|m\rangle\langle m|p_z|o\downarrow\rangle + \langle o\downarrow|p_y|m\rangle\langle m|p_z|o\uparrow\rangle\right\}$$

TEMPERATURE DEPENDENCE OF THE ESR SIGNAL

The conduction band of CdS is known to be close to $\vec{k}=o$ and has Γ_7 symmetry.(2) This symmetry has been determined from both experiment and band structure calculations. The Γ_7 states transform under the symmetry operations of the crystal like the spin-states of an electron. Therefore Hopfield(3) has written the

effective mass Hamiltonian as

$$H(\vec{k}) = \begin{bmatrix} Ak_\perp^2 + Bk_z^2 & iCk_+ \\ -iCk_- & Ak_\perp^2 + Bk_z^2 \end{bmatrix}$$

where $k^2 = k_x^2 + k_y^2$ and $k_\pm = k_x \pm ik_y$ The c-axis is taken to be the z-direction. This Hamiltonian yields an expression for the energy of the conduction band edge in CdS

$$E(\vec{k}) = (Ak_\perp^2 + Bk_z^2)I + C(k_x\sigma_y - k_y\sigma_x)$$

where σ_i are the Pauli matrices. This implies that the Kramers degeneracy is lifted away from k=o. If a Zeeman term is then added and the spin-dependent part diagonalized one can write down the conditions for ESR of the conduction electrons.

$$\epsilon(\vec{k},\vec{s}) = 2C(k_x s_y - k_y s_x) - g\mu_\beta \vec{H}\cdot\vec{S}$$

the secular equation becomes ($s=\frac{1}{2}$):

$$\begin{vmatrix} -\frac{1}{2}g\mu_\beta H - W & -iCk_- \\ iCk_+ & \frac{1}{2}g\mu_\beta H - W \end{vmatrix}$$

yielding

$$W = \pm\frac{1}{2}\sqrt{(g\mu_\beta H)^2 + (2Ck_\perp)^2}$$

The transition energy then becomes

$$h\nu = \sqrt{(g\mu_\beta H)^2 + (2Ck_\perp)^2}$$

This means that the position of the resonance will be dependent on $k_\perp$ and hence could be temperature dependent. Since under normal conditions at low temperatures the

electron gas is degenerate, the Fermi level and g-value are independent of temperature. Thus even if the change in $k_\perp$ is small, one might expect to observe it.

On the other hand if $2Ck_\perp \ll h\nu$ the effect could give a change in the line shape. Since on expanding

$$H \approx \frac{h\nu}{|g\mu_\beta|} - \tfrac{1}{2}\frac{(2Ck_\perp)^2}{|g\mu_\beta| h\nu}$$

For samples containing 10^{17} electrons per cm^3 one can estimate the magnitude of the second term using $k_F \approx k_\perp$ and $N = \frac{2}{(2\pi)^3}\frac{4\pi k_F^3}{3}$. This gives $k_F = 1.44 \times 10^{-3}$ cm^{-1}, $E_F = \frac{\hbar^2 k_F^2}{2m^*} = 4 \times 10^{-3}$ eV $\sim 45^\circ$K. Hopfield using his optical data has placed an upper limit on the value of $C = 6 \times 10^{-11}$ eVcm.

Thus in going from K_a-band (34GHz) to X-band (9GHz) an increase in the line width of a factor of three is predicted.

Recent measurements on the temperature dependence of the g-value in III - V compounds, InAs[4] and InSb[5], were made at temperatures comparable to or higher than that calculated for the Fermi level at a concentration of $N = 1.4 \times 10^{14}$ cm^{-3}. ($T = 7.2^\circ$K) This temperature variation was not completely understood and

a mechanism was proposed that such a behavior could be explained by a variation of the Fermi level with temperature due to condensation of part of the free carriers on shallow impurity levels.

The g-value in InAs varied linearly with temperature from 4.2°K to 25°K at 0.14% (i.e. Δg = 0.14 as ΔT = 10°K). A rough measurement by Slagsvold[6] at 35GHz indicated that Δg for Cds:I was of the same order of magnitude (Δg = 0.001 for ΔT = 2.6°K).

In view of these facts it seemed very worthwhile to study the temperature variation of the g-value of CdS:I in greater detail, and to compare the line width of the ESR signal at 35GHz and 9GHz.

CHAPTER 3

SYSTEM DESCRIPTION

A complete block diagram of the electron spin resonance spectrometer which was used for this thesis is given in Fig. 1. Straight crystal detection with field modulation synchronized with a lock-in amplifier were used in conjunction with a magic tee microwave bridge. Dewars are also shown, in a schematic way, to indicate that the sample was cooled to liquid helium temperatures. In order to fix the frequency of the klystron at the resonant frequency of the microwave cavity, an automatic frequency control (AFC) was connected to the reflector voltage of the klystron. This device is discussed in detail later in this chapter.

Field measurement was accomplished by means of a nuclear magnetic probe (NMR) using a glycerin sample. The NMR signal was detected by means of a marginal oscillator and fed into the lock-in amplifier in parallel with the ESR signal.

The klystron frequency was measured by beating the microwave frequency with the frequency of a transfer oscillator, which was oscillating typically at around the sixtieth harmonic. The frequency of the transfer oscillator was then measured with the Hewlett Packard counter, which was used also to measure the frequency of the NMR oscillator.

The magnet power supply was a Magnion Model HS 1365B with a rotating coil field probe, and the magnet

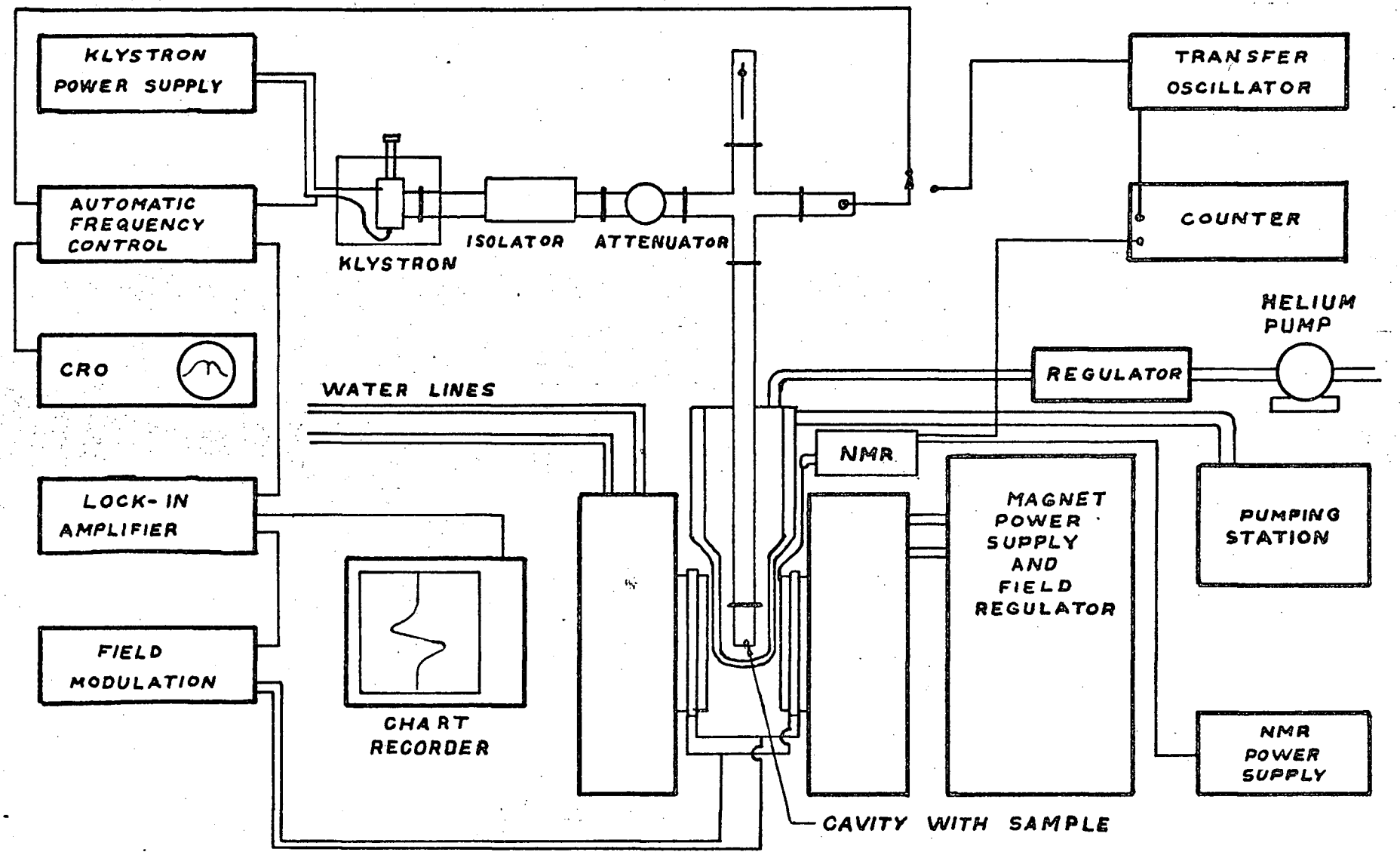

Fig. 1 Block Diagram

was a 9½" diameter, 2" pole gap Magnion magnet. The crystal detector was a Microwave Associates 1N23B low noise diode.

On the oscilloscope is shown a sweep of a klystron power mode with a sharp dip in power due to the absorption of power at the resonant frequency of the cavity.

TEMPERATURE CONTROLLED DEWAR

The temperature controlled dewar, as shown in Fig.2, consisted of a top section containing the liquid nitrogen and liquid helium reservoirs and a bottom section containing the microwave cavity and temperature control apparatus. The top section, with an outer liquid nitrogen reservoir made of brass and an inner liquid helium reservoir made of stainless steel, was constructed roughly along the lines of other metal dewars used in this group for infra-red experiments. The main departure from this design was the use of a hanging helium reservoir so that the position of the dewar tail could be adjusted to coincide with the microwave input in the bottom section. Adjustment was done by means of three adjusting screws located on the top plate of the dewar with a brass bellows acting as a flexible vacuum wall. Another feature of the helium dewar was the stainless steel wave guide which acted as the dewar tail. This tube was

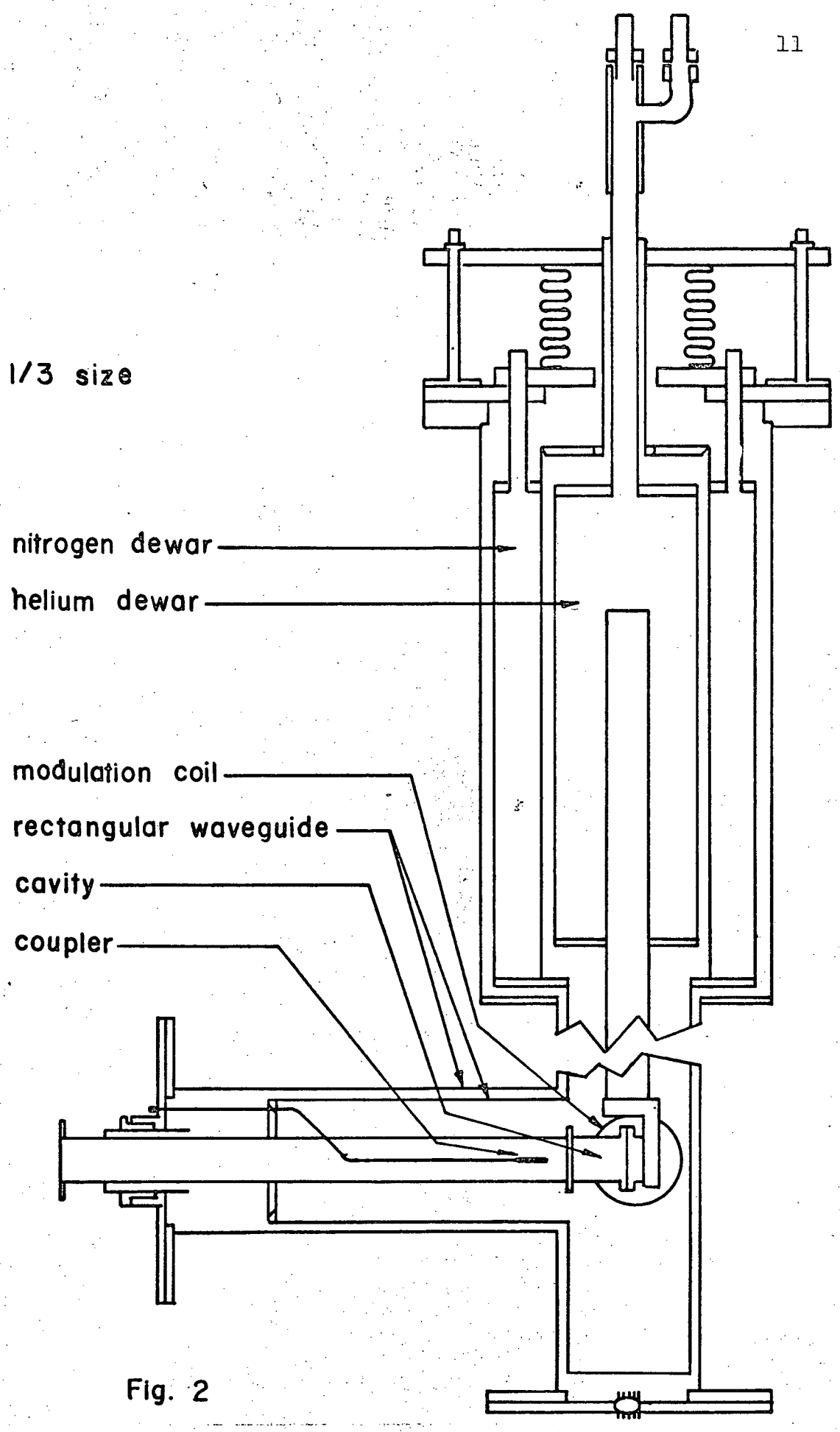
1/3 size
nitrogen dewar
helium dewar
modulation coil
rectangular waveguide
cavity
coupler

Fig. 2

allowed to project about halfway up into the center of the helium dewar. This was to allow work to be done both at low temperatures while the helium could overflow into this tube, and at higher temperatures when the helium in the tube boiled away leaving the tail isolated from the reservoir. This arrangement is similar to one used by MacPherson[7] in a dewar designed for infra-red experiments.

The bottom section of the dewar was designed to allow for the introduction of the microwave signal from a horizontal direction and at the same time to provide sufficient heat shielding and thermal isolation for operation down to liquid helium temperatures (4.2°K). In order to do this, it was necessary to have an outer vacuum wall, a liquid nitrogen radiation shield and the X-band wave-guide and cavity within the 2" pole gap of the available 9½" Magnion magnet. This problem was solved by using large size extruded brass waveguide as the outer vacuum wall and radiation shield. The extruded brass gave a good vacuum tight wall and fit snugly into the pole gap while size 3"x1.5" waveguide was the radiation shield allowing plenty of room for the microwave and temperature control apparatus.

The microwave power was fed to the cavity through Type 304 stainless steel waveguide with a wall

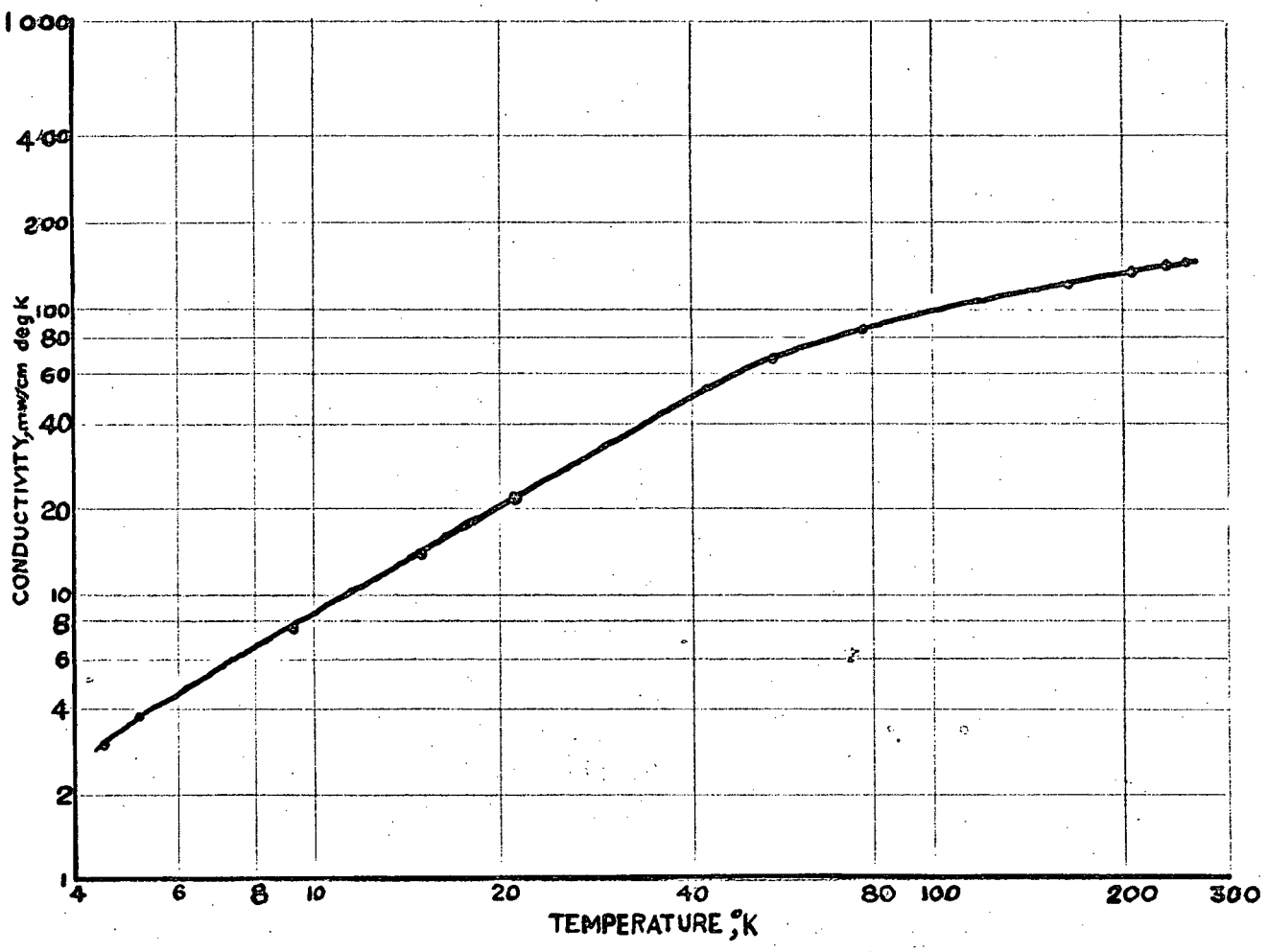

Fig. 3 Thermal Conductivity of Type 304 Stainless Steel

thickness of 1/100". This waveguide was chosen to provide good thermal isolation between the cavity at helium temperatures and the outer wall at room temperature. In Fig. 3 is shown the curve giving the thermal conductivity versus temperature curve for this type of stainless steel. Below, in Fig. 4 is shown the curve of length of waveguide needed to maintain a 4.0°K to 80°K temperature difference as a function of the conductive heat leak for this waveguide. This curve was obtained by numerical integration of the conductivity curve according to the following scheme:

$$L = A/\dot{Q} \int_{T_1}^{T_2} K(T)\, dT$$

Another source of conductive heat leak between room temperature and sample temperature was the assembly of electrical leads necessary to operate the thermometer and the heater. This heat source was minimized by wrapping the wires around the helium tail several times so that the heat leak would be fixed to the dewar tail rather than be allowed to propagate to the sample holder. A more reliable way to short circuit this heat leak would be to have the

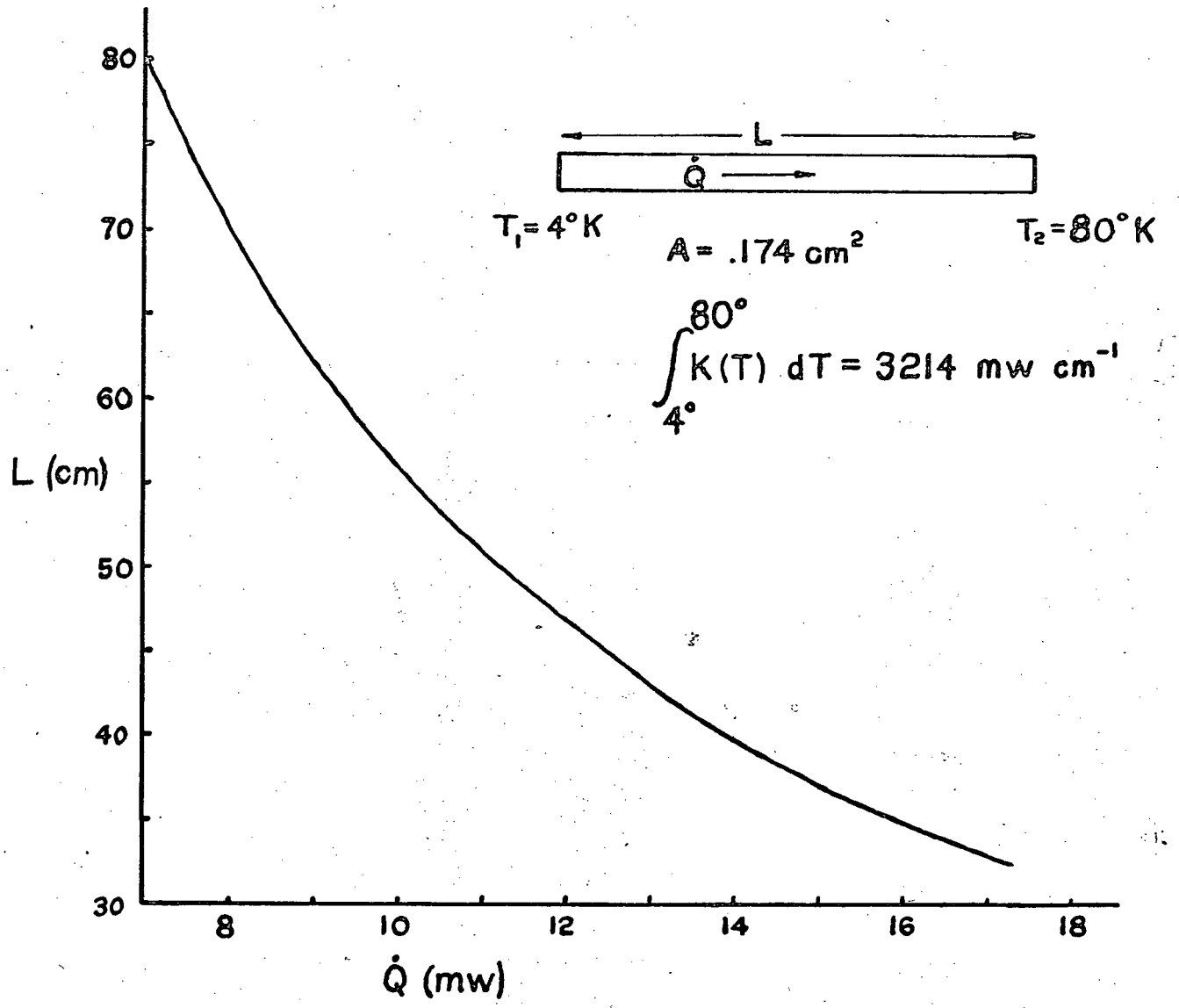

Fig. 4 Waveguide Length Curve

wires pass through the helium reservoir. However, if the wires leading to the thermometer were held at the temperature of the helium reservoir, the thermometer would give an unreliable reading at higher operating temperatures because of the regulating effect of these wires on the thermometer itself. Therefore, the former method was used. Also, since the thermometer wires carried only a small current, it was possible to use low thermal conductivity, 72 ohms per ft. constantan wire.

The use of both a brass radiation shield and a brass dewar presents a considerable radiative heat leak. The total low temperature emissivity of polished brass is given by the Handbook of Chemistry and Physics as 0.60 while that of silver is 0.02. * Therefore, sixty per cent of the power radiated to the cavity will be absorbed by the brass. Similarly, the power radiated by the brass shield at 77°K will be sixty percent of the black body radiation at that temperature. This results in a heat leak of about 2 milliwatts which could be almost completely eliminated by using silvered surfaces.

Shown in Fig. 5 is a detailed picture of the microwave cavity with the bottom of the helium dewar attached. The cavity was split at the three quarter mark along its length and the end piece, which acted

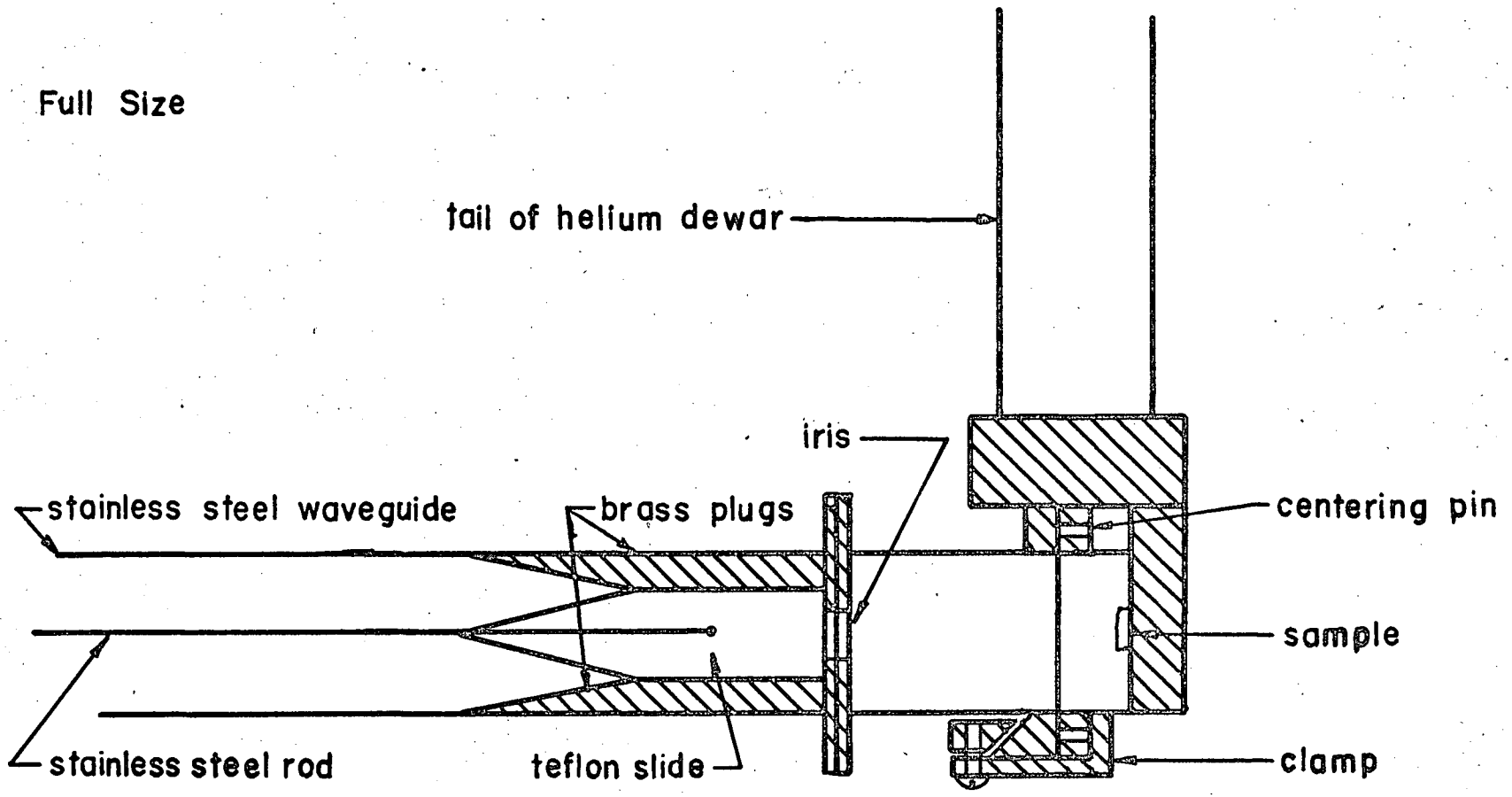

Fig. 5

Cavity Assembly

as sample holder, was soldered to the helium dewar tail. This was done in order to assure a good thermal contact between the sample and the dewar tail. The front and back parts of the cavity were then fitted together by means of centering pins and clamped into position, with the clamp shown. The cavity quality factor (Q) did not suffer appreciably from the use of this technique, but sample changing was made more difficult since it then necessitated removal of the helium dewar.

In the waveguide immediately in front of the cavity was a coupling device using a teflon slider operated from outside the dewar by means of a stainless steel rod. On either side of the slider were brass plugs which, when the slider was pulled back, carried the waveguide into the cutoff region effectively decoupling the cavity. The higher dielectric constant of the teflon($\epsilon \sim 2$) was sufficient to bring the waveguide out of cutoff and progressively couple the cavity as the slide was pushed toward the cavity iris. By coupling and de-coupling the cavity in this way, it was possible to distinguish the power absorption dip due to the cavity from spurious reflections due to discontinuities in the microwave circuit. This facility was particularly useful when the cavity Q was reduced by a "lossy" sample. During the course of the experiment, the slider was left

in the optimum coupling position as determined by sharpness of the cavity Q.

Magnetic field modulation was originally to be provided by means of external coils wound about the poles of the magnet. However, this design proved inadequate in that, owing to the skin depth of the metal walls of the dewar and cavity, the modulation field could not penetrate in sufficient strength to the sample. Therefore, new modulation coils were wound and mounted immediately adjacent to the cavity on the radiation shield. Also, the cavity walls were milled down in order to further enhance the field strength reaching the sample inside the cavity.

However, the force exerted on the modulating coils by the static magnetic field was transmitted to the radiation shield in the form of mechanical vibration. This vibration, propagating to the split cavity, caused noise to be introduced into the signal which varied quite distinctly with modulation strength. Various modulation frequencies were tried but none was found which appreciably diminished this vibration. In spite of these difficulties, it was possible to operate the modulation coils below a threshold power beyond which the noise increased rapidly.

As was previously mentioned, the temperature controlled dewar did not reach the desired temperature of 4.2°K but stayed at about 12°K when helium was in the dewar tail. Under maximum pumping speed, the lowest attainable temperature was 5.2°K as measured by a Solartron calibrated thermometer. A number of changes could be made in order to improve this low temperature performance in order to operate efficiently in the 4.2°K to 12°K range.

First of all, the cavity and dewar tail assembly could be silver plated in order to reduce the radiative heat leak previously mentioned. Also a polystyrene plug placed in the stainless steel waveguide would reduce thermal radiation to the cavity assembly from the room temperature waveguide. These modifications would minimize the radiative heat leak.

In order to minimize the conductive heat leak, all electrical leads should pass through the helium dewar and exit from the dewar through the helium return pipe. Also, a baffle system could be incorporated into the helium dewar to circulate the helium gas around the outer wall of the liquid helium container. In addition to reducing the heat leak, this arrangement makes more efficient use of the cold helium gas.

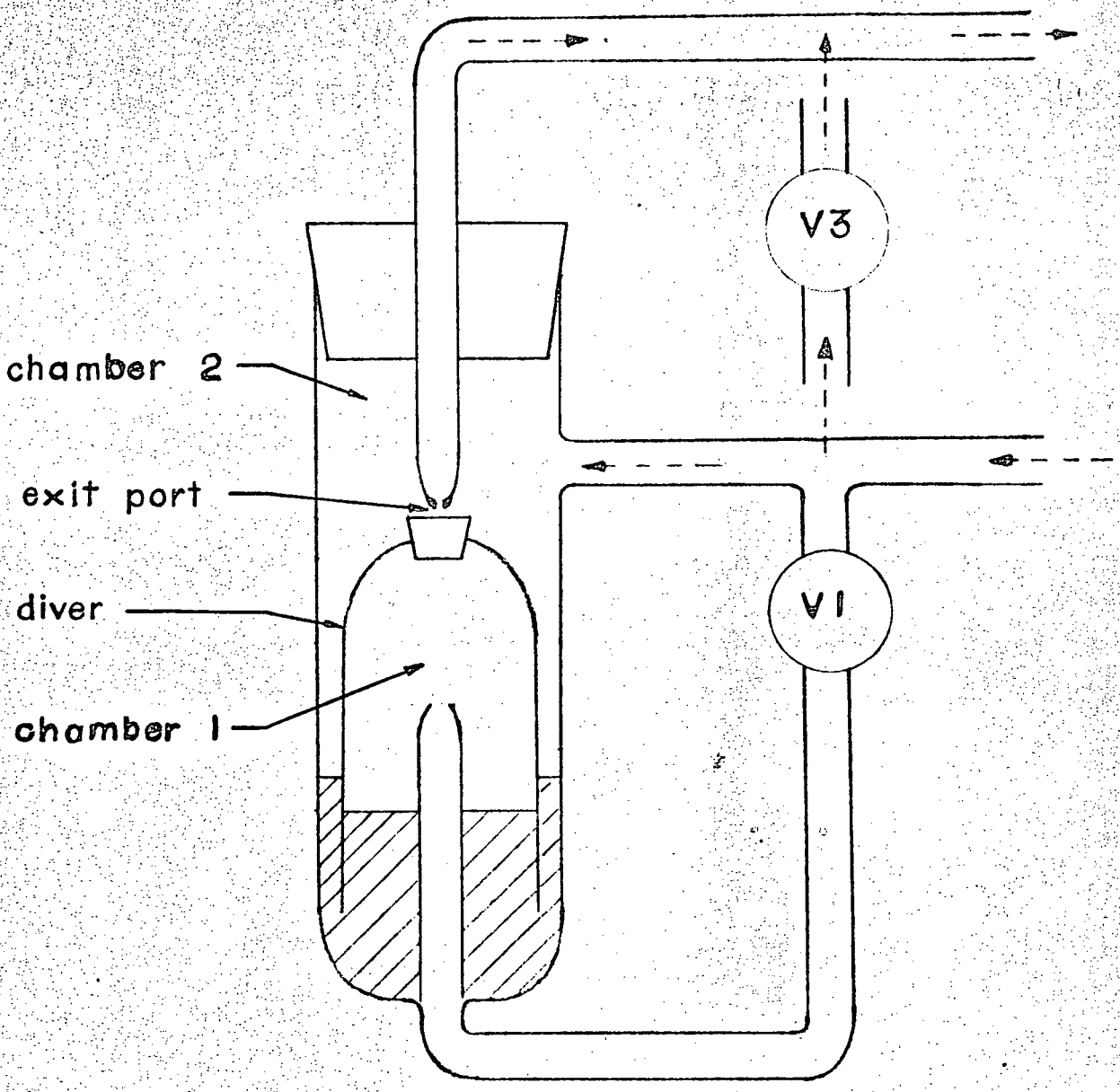

Fig. 6 Pressure Regulator

Temperature control at low temperatures was provided by a helium pumping apparatus which incorporated a pressure regulator. This regulator is shown in Fig. 6. Valve No. 1 was left open until the desired pressure was reached by pumping on the helium reservoir. When valve No. 1 was closed, this reference pressure was locked in chamber No. 1, and the regulator would always return to that pressure through the following process. Any decrease in pressure beyond the reference pressure caused the diver, which was floating in mercury, to rise, thus blocking the exit port from chamber No. 2. When the helium pressure from the reservoir again increased the diver would move down and away from the exit port allowing more helium to be pumped until the reference pressure was again attained. In practice, the diver should reach an equilibrium position allowing a steady rate of helium pumping. This condition is critically dependent of the size of the exit hole and the rate of helium pumping. An exit hole of one millimeter was found adequate when coupled with a shunting valve (Valve No. 3) to accomodate higher pumping rates

GLASS DEWARS

Fig. 7 shows the glass dewar arrangement utilized in obtaining signals in the 4.2°K to 1.7°K

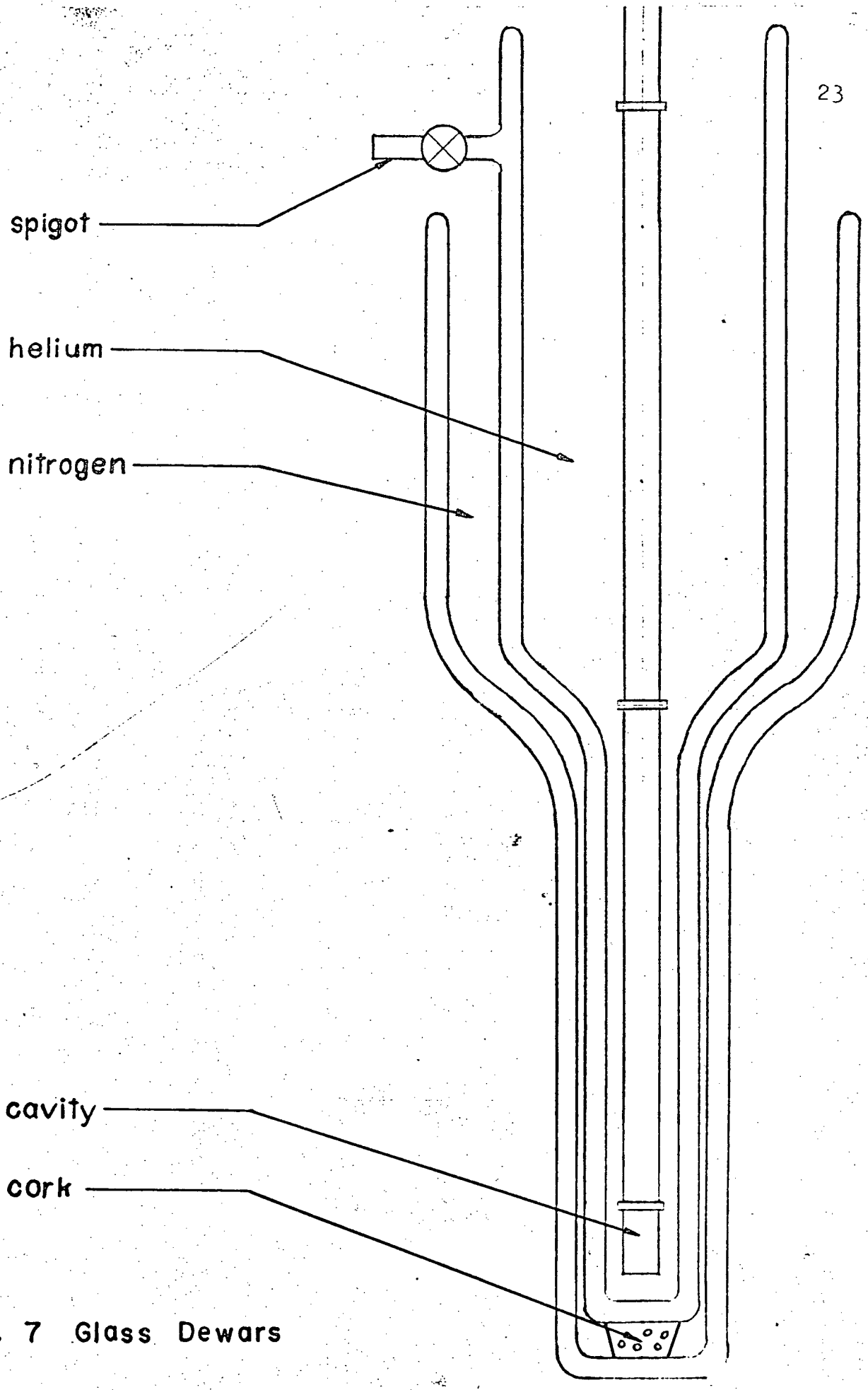

Fig. 7 Glass Dewars

temperature range. This arrangement consisted of two separate dewars, the inner one containing liquid helium and the outer one containing liquid nitrogen, and thereby supporting the liquid helium dewar in a liquid nitrogen bath. Both of these dewars were silvered on the inside walls except for two narrow strips through which their levels could be observed. A permanently evacuated wall was used in the nitrogen dewar whereas the helium dewar was equipped with a spigot through which its wall was flushed and pumped before each run. The microwave power was fed to the cavity through the same kind of thin walled stainless steel waveguide as was used in the metal dewar. However, in this design, the liquid helium was allowed to fill the waveguide and cavity immersing the sample to provide good temperature homogeneity.

Work was first done at the higher temperature of 4.2°K just after the helium dewar was half-filled because the heat leak down the waveguide was too great to allow effective pumping. Only when the helium level had descended below the narrowing in the dewar was it possible to operate at a pumped helium temperature of 1.7°K. This was partly because of the greater thermal isolation from the room temperature dewar head and partly because the flange just above the narrowing

acted as a partial radiation shield.

One disadvantage of having the cavity immersed in liquid helium in this way was that the helium bath became cooler as the level descended. Temperature variation in susceptability and density of the helium then caused a cavity frequency drift which though small, had to be corrected for in the analysis of the data. For example, J. Wilks[6] gives the rate of change of the density of He^4 at 1.7°K as .007%/°K.

THE AUTOMATIC FREQUENCY CONTROL

An automatic frequency control (AFC) unit was used to stabilize the klystron at resonant frequency of the cavity, so that a proper absorption signal could be obtained. This was accomplished by a device, similar to a Varian design, utilizing the fact that the frequency of a reflex klystron could be adjusted by variation of the reflector voltage. Therefore, by applying a correction voltage to the reflector proportional to the difference in the actual frequency and the frequency corresponding to the minimum of the power dip caused by the resonant cavity, the frequency was kept at the frequency of the cavity.

The power curve with the klystron mode and cavity power dip was detected from the crystal rectifier on one arm of the microwave bridge, and displayed on the oscilloscope as shown in Fig. 1 . The reflector voltage was then adjusted so that the klystron frequency was near the bottom of the power dip when the reflector voltage modulation was turned off. Once the frequency was adjusted close to the cavity frequency in this way, it became possible for the AFC to "lock-on" to the power minimum in the following way.

The AFC had its own internal 10kc oscillator which applied a small amplitude voltage to the reflector. This oscillator is seen in the lower left hand side of the circuit diagram in Fig. 8. Depending on which side of the power dip the frequency of the klystron happened to be,

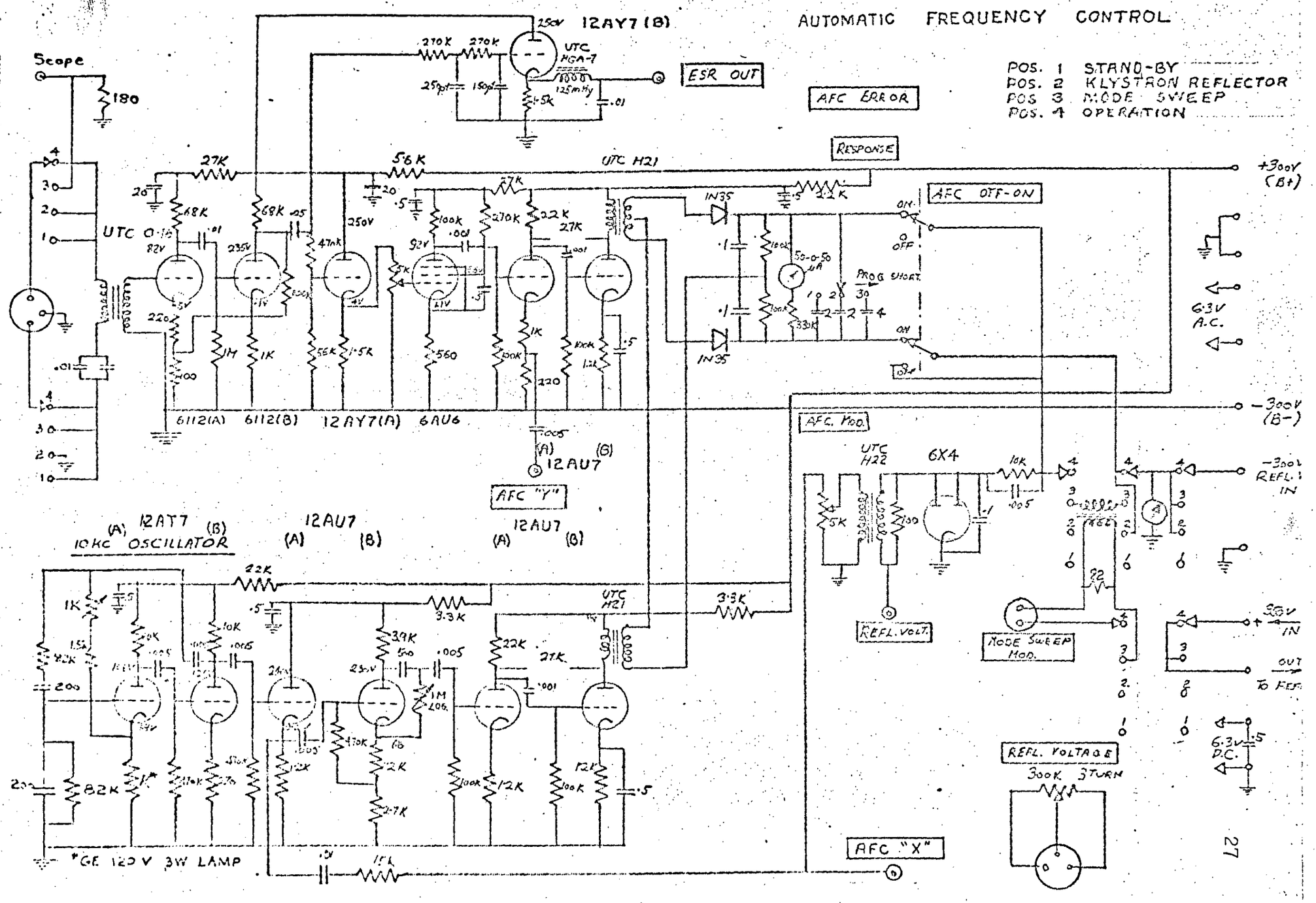

Fig. 8 A. F. C. Circuit Diagram

a signal would be received which was either in phase or out of phase with the modulation. This phase condition was detected with a diode and capacitor circuit shown near the middle of Fig.8, which also rectified the difference signal and applied it as a correction to the reflector voltage. This voltage was applied in such a way as to hold the klystron to the power minimum as detected by the crystal. If the microwave bridge was balanced correctly, this minimum would correspond exactly to the cavity resonant frequency and the AFC would cause the klystron to follow the cavity as its frequency shifted due to the dispersion signal at resonance. In this way the dispersion signal would be cancelled out and the signal given by the spectrometer would be a pure absorption signal.

The ESR signal itself was taken after the second stage of amplification to a cathode follower seen at the top of the circuit diagram, with an inductive output to filter the 10kc modulation from the signal. It was then fed to a "lock-in" amplifier where it was phase detected at a 400 cps modulation frequency corresponding to the magnetic field modulation frequency.

The description of the AFC up to this point has been of the "locked-in" position. Three other modes of operation were available for convenience of operation and a number of outputs were also present, as indicated on the

circuit diagram. Briefly, these operating modes were:

3. - Mode Sweep Operation which placed a 60cps voltage on the reflector of the klystron thus modulating the microwave frequency and giving a 60cps output at the crystal detector. This was fed to an output jack which could be attached to an oscilloscope enabling one to observe the klystron mode:

2. - Klystron Reflector which was a special safety switch to make sure that the reflector voltage was turned on before the klystron beam voltage.

1. - Stand-by which switches off the reflector voltage.

SENSITIVITY

According to Feher's comprehensive article[8] on the sensitivity of electron spin resonance spectrometers, the ultimate sensitivity of the straight crystal detection scheme is about 10^{12} spins. For a variety of reasons, the spectrometer used in this experiment was considerably less sensitive, the highest sensitivity obtained being about 5×10^{14} spins. This figure was calculated by measuring the signal to noise ratio of a weighed sample of dpph (di-phenyl-picaryl-hydrazyl) and assuming one unpaired spin per dpph molecule.

The main factors contributing to loss of sensitivity were crystal noise in the diode detector (1N23B), grounding problems, and noise introduced by the AFC. Crystal noise can be minimized by use of a higher modulation frequency, typically 100kc, since crystal noise varies approximately as the inverse of $\sqrt{f}$. However, a higher frequency of field modulation introduces skin depth problems, especially in a metal dewar, and necessitates the construction of special thin walled cavities such as those described in Poole[9]. Since this was not suitable, a modulation frequency of 400 cps was used.

The noise introduced by the AFC in its function of modulating the reflector voltage of the klystron and application of a correction voltage was

mainly high frequency noise and did not have a great effect with the lock-in amplifier detecting the signal at 400 cps. The same argument can be applied to the 60 cps. ground noise which should have been filtered out by the lock-in amplifier.

LINE SHAPE

There are many factors which influence the line shape of an ESR signal. Among these are spurious broadening effects due to the conditions under which the ESR spectrometer is operating and one must minimize or compensate for these effects before meaningful information can be gathered from line shape data.

The first and most obvious consideration is modulation broadening caused by using a field modulation so high that it exceeds the natural line width of the signal being measured. As a result, the signal received is averaged over both sides of the line when the field is at its resonant value. Therefore, apart from distorting the shape of the wings of the signal, the overmodulation will shift the half-power peaks apart making the line appear broader than it actually is. Since the line width is a very important parameter in the determination of relaxation times, it is necessary to keep the modulation below the distortion level. Serious distortion occurs when the modulation amplitude exceeds the difference in field between the peaks of the derivative curve. For more detailed measurements on the shape of the line, the modulation must be further reduced.

Care must also be taken to make sure that the power level is not too high since the spin system must be

able to continuously relax to its equilibrium state. If the power level is so high that the spin system is in a very excited state as the signal is detected, a broadening of the line results which varies as the square root of the power. No such saturation effects were apparent in any of the samples used for these experiments.

A third instrumental broadening to be considered here is the broadening due to the inhomogeneity of the static magnetic field used. If the spread in field across the volume of the sample is of the order of the line width of the signal, then a broadening will result because different parts of the sample will experience different fields. For example, with a line width of about 3 gauss and a resonant field of about 10 kilogauss, the magnetic field should be homogeneous to one part in 10^5 over the volume of the sample. This is not too difficult to achieve with samples typically .1 cc in volume.

Fig. 9 shows a trace of a typical derivative curve of a CdS(I) ESR signal. The sensitivity is low as shown by the noise arrow, because the field modulation is kept small in order to prevent distortion. From this derivative signal the absorption curve was obtained by integration and is shown in Fig. 10. It is of interest to know whether this curve is Gaussian or Lorentzian in shape in order to determine the form of the Hamiltonian.

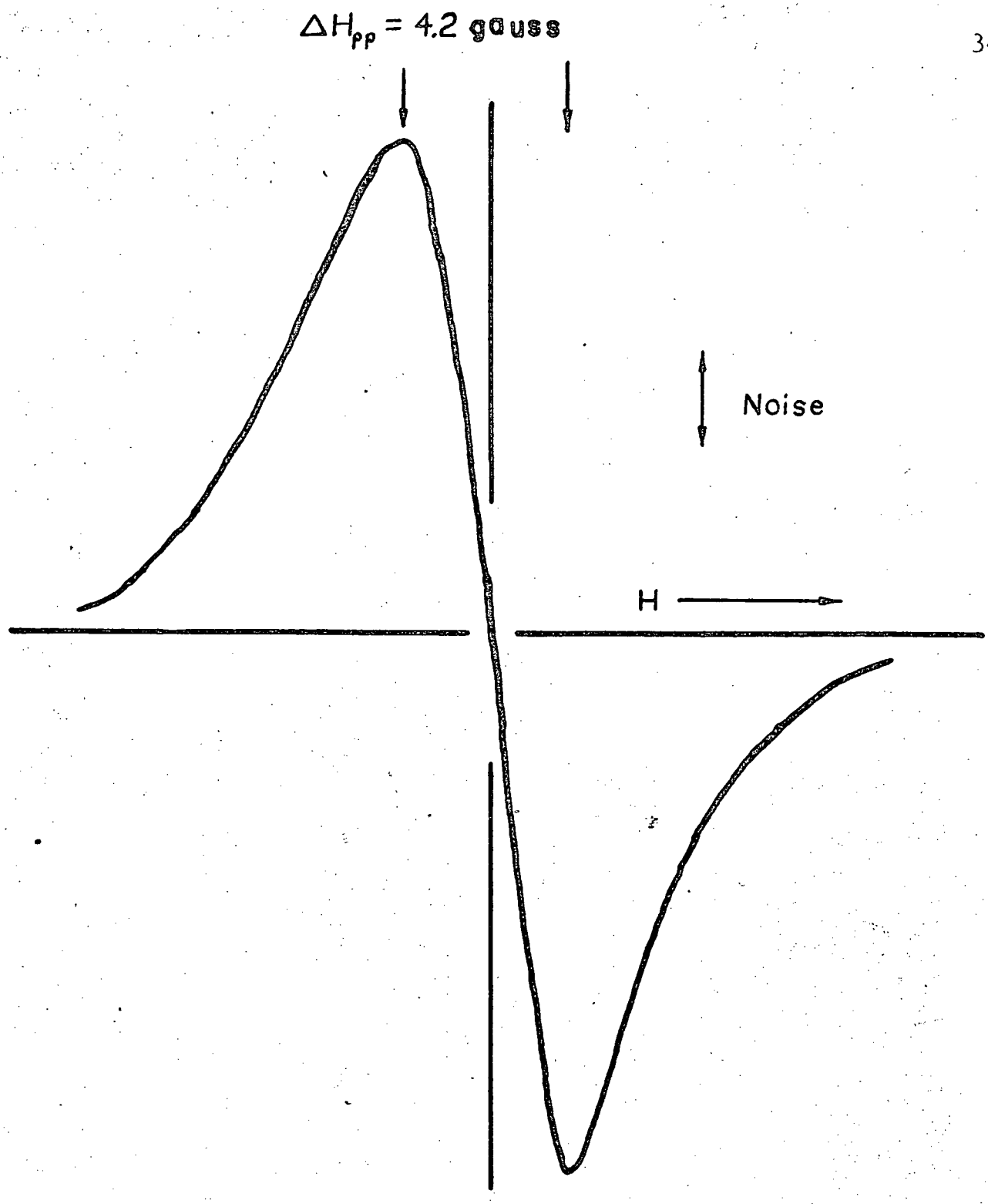

Fig. 9 CdS: I Derivative Signal

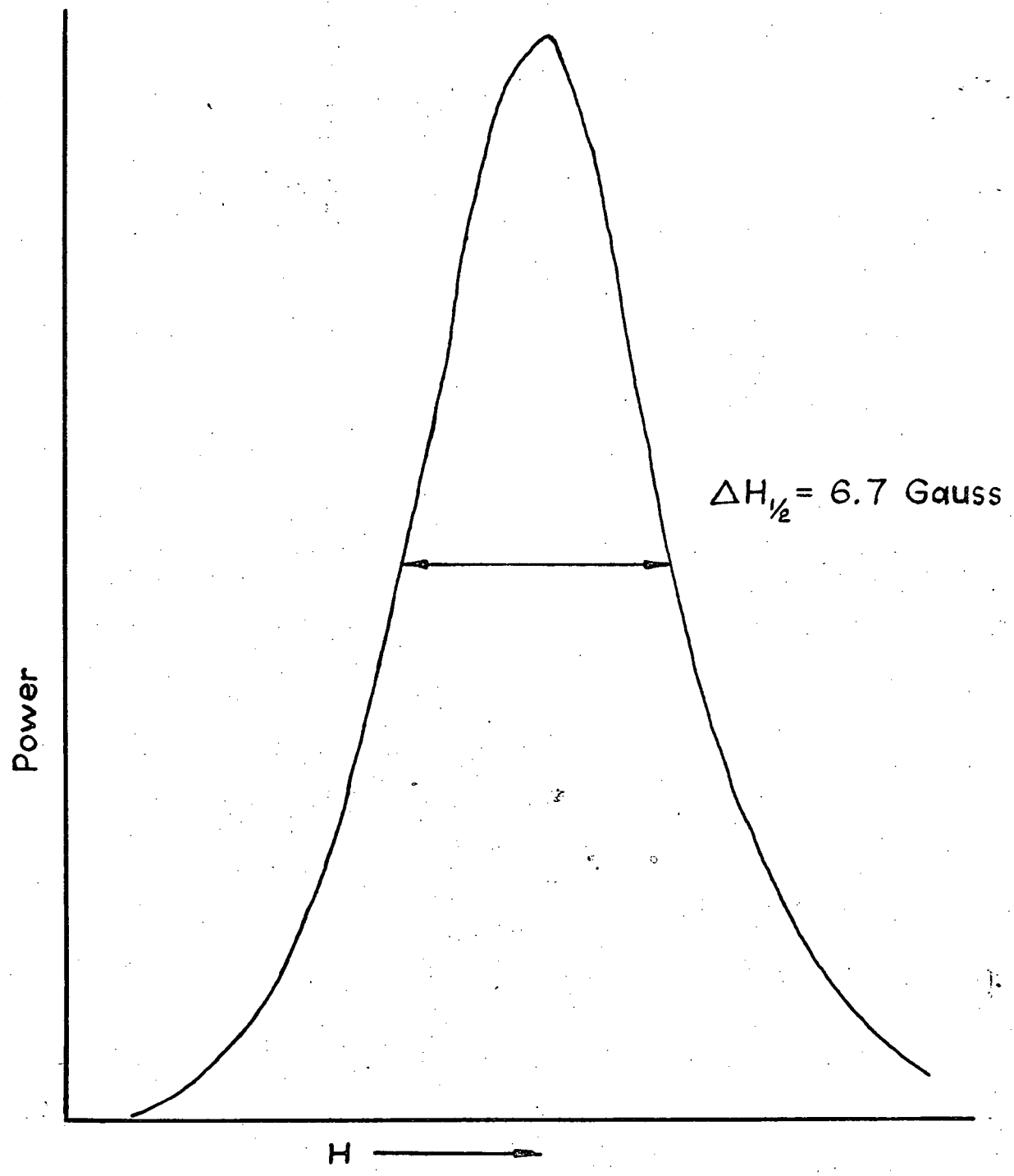

Fig. 10 CdS:I Absorption Curve

However, close examination of these curves will show that there is an assymmetry about the origin which is characteristic of neither of these shapes.

Further study is required to explain this assymmetry and it will be undertaken in this laboratory. However, the ratio of half power line width ($\Delta H_{\frac{1}{2}}$) to peak to peak line width (ΔH_{pp}) is 1.6 which is typical of a Lorentzian curve. It may be that the assymmetry was caused by an admixture of dispersion signal but our signal-to-noise ratio was not sufficiently high to study such refinements.

CHAPTER 4

EXPERIMENTAL PROCEDURE

Samples of CdS were originally selected for a low temperature run by observing their effect on the Q of the microwave cavity at room temperature. In effect this is a measure of their conductivity, a poor cavity Q meaning a high conductivity indicating a high doping. The sample was placed in the bottom of the detachable end piece of the cavity where the microwave magnetic field was strong. The sample was fixed in its position by pressing in a snugly fitting piece of polystyrene foam which also contained a piece of dpph for a reference signal. The assembled cavity was then wrapped in tape to prevent scratches on the glass dewar. When the glass dewar was put in position, a seal with the top plate and helium return system was made by pulling a rubber sleeve over the top of the glass. The nitrogen dewar was then put under the helium dewar, making contact through a cork buffer at the bottom. The helium dewar wall was then flushed twice with nitrogen gas and nitrogen gas at atmospheric pressure was left in as an exchange gas. The inside of the dewar was also pumped out and helium gas was put in so as not to contaminate the helium which would be added later. Liquid nitrogen was then poured into the outer dewar and

the system was left for about an hour to reach temperature equilibrium through the exchange gas. The helium dewar wall was then pumped with a roughing pump to a suitable pressure for cryopumping and then was sealed off. Liquid helium was added through the top plate of the dewar by means of a flushed transfer syphon with evacuated walls. The level of the helium was monitored through a narrow vertical gap in the silvering of the dewars. The helium could then be left to boil off at atmospheric pressure. It was convenient to fill the helium dewar only about half way since above this level the helium boiled away very quickly.

At times a heat leak would develop between the helium and nitrogen sections. This was thought to be due to helium gas leaking into the helium dewar wall through minute cracks or scratches in the glass which would usually seal themselves at lower temperatures. It would not be possible to cryopump this helium gas by condensing it at liquid helium temperature as is possible with nitrogen gas. Therefore, the gas would remain in the space between the liquid helium and liquid nitrogen and provide a sufficient heat leak to prevent a successful transfer. Sometimes reflushing after a suitable waiting period would result in a successful second try.

EXPERIMENTAL RESULTS

The strongest signal was obtained from a highly doped sample of CdS(I) from the Ford Laboratories. Usingthis sample and the commercial NMR probe previously mentioned, sufficient accuracy was obtained for a measurement of the expected g-shift. Shown in Fig. 11 is a sample trace from such a run with a time constant of one sec. and chart speed of 2" per minute. The sharp vertical field markers were artificially produced markers superimposed on the signal and represent the NMR field calibration. The accuracy in the linearity of these field measurements is indicated by the line drawn through the points of the plot of field versus time plotted directly on the experimental chart. The field modulation in this example is approximately half the line width of the ESR signal.

Shown in Fig.12 is a broad trace of the spectrum of CdS(I) with its single resonance line at a g-value of 1.782. From previous work done by B.J.Slagsvold, it is known that the g-value ranges from 1.767 for H perpendicular to the c-axis of the crystal to 1.785 for H parallel to the c-axis of the crystal. The broad resonance seen at the low g-value end of the spectrum was believed to be an effect caused by impurities in the cavity rather than by any properties of the sample, but this is under further study.

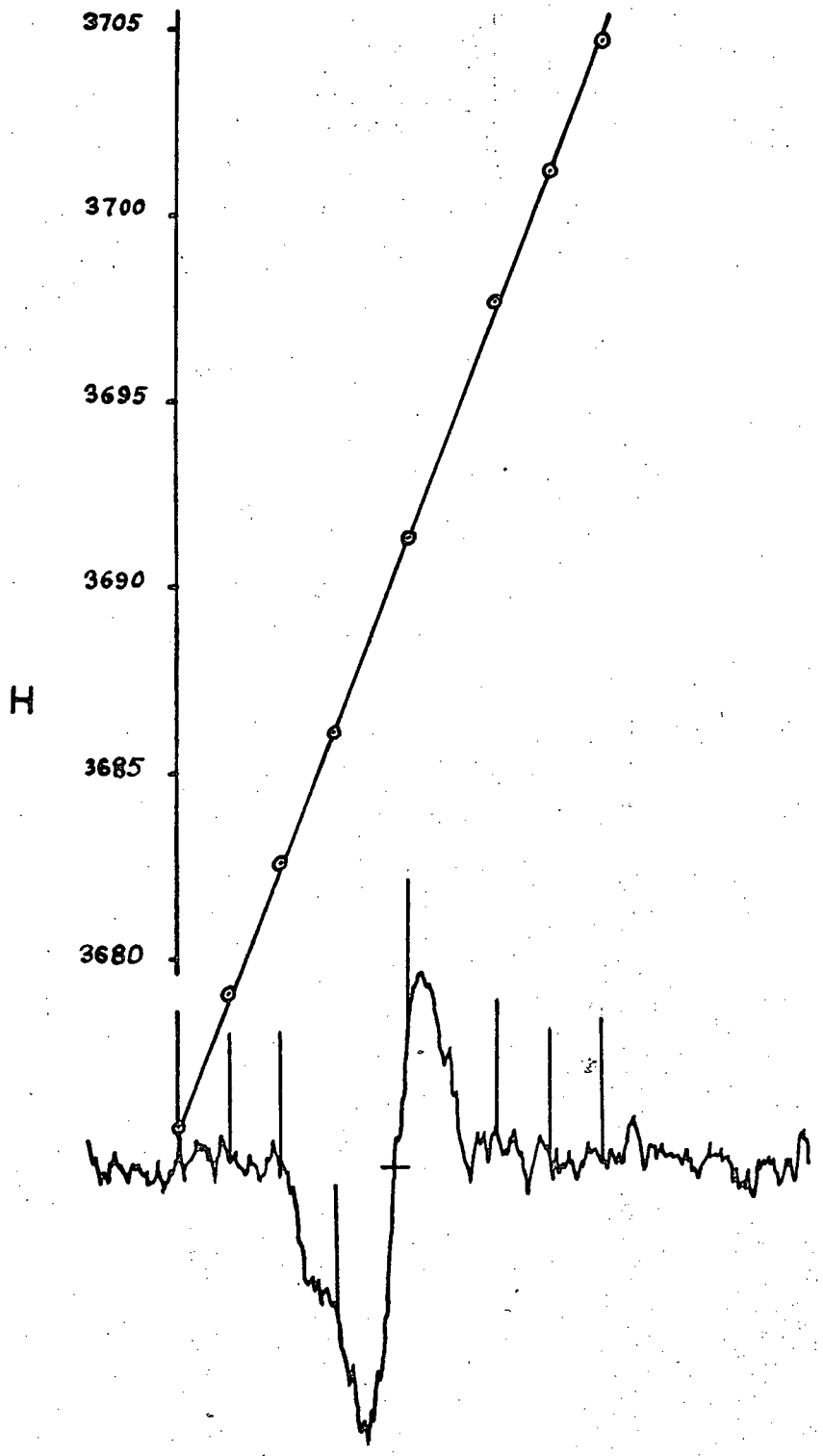

Fig. 11 Experimental ESR Signal of CdS:I

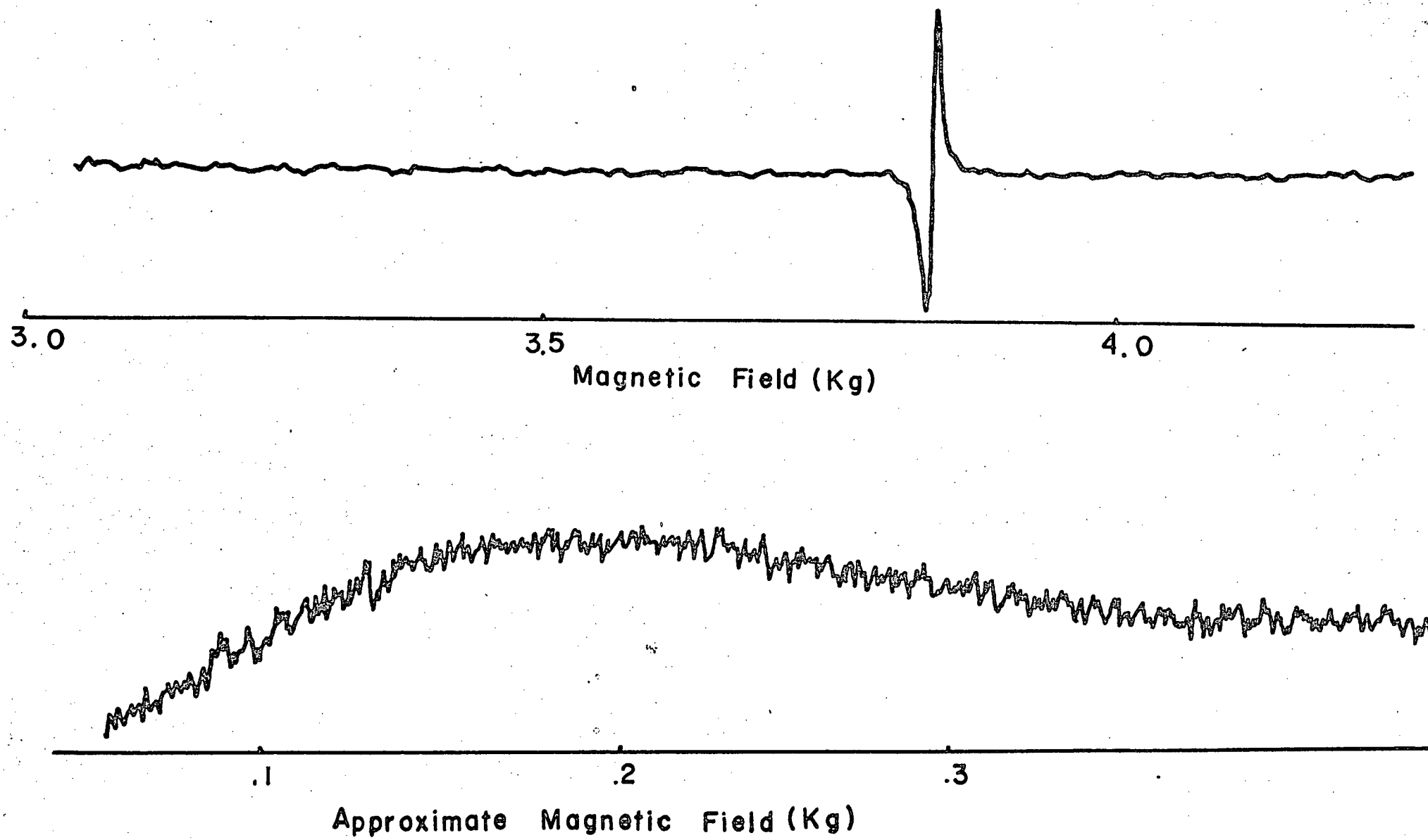

Fig. 12 Broad Trace of Spectrum and Low Field Signal

In the determination of the expected g-value shift in the range from 1.7°K to 4.2°K, five figure accuracy was required. Experimentally, this meant that the magnetic field and the klystron frequency had to be determined to the same five figure accuracy. Of these, only the magnetic field determination presented difficulty.

This difficulty was due in large measure to the fact that the magnetic field modulation was common to both the ESR and NMR detection systems even though the NMR line was considerably narrower than the ESR line. Because of the weakness of the ESR signal it was desirable to modulate the field to a amplitude high enough to give a sufficient signal to noise ratio for accurate work. But, since the narrower NMR signal was in the same field, it would be necessary to over-modulate this line to the point of distortion. Lack of space in the glass dewars prevented the relocation of the modulation coils inside the dewars themselves. Also, previous experience with noise from internally mounted modulation coils led away from this method.

This problem was eventually overcome by the use of a commercial NMR probe with its own modulation coils operating at a frequency different from that of the main field modulation. Even with this innovation

however, the main field modulation could not be operated at a very high level without introducing a great deal of noise on the commercial NMR signal.

CALCULATION OF G-VALUE

The g-value was calculated from the formula:

$$g = h\nu/\beta H$$

h = Planck's constant = 6.62517 erg-sec

ν = microwave frequency

β = Bohr Magneton = 9.2731 $\frac{\text{erg}}{\text{gauss}}$

H = magnetic field

The relationship between the NMR oscillator frequency (f_{NMR}) and the magnetic field was taken as

$$H = 2.3487 \times 10^{-4} \; f_{NMR}$$

The magnetic field at the ESR signal was obtained by drawing a graph of field vs. time using the field marker points produced by the NMR signals. The point where the ESR line crossed over the baseline as shown in Fig.11 was taken as the position of the ESR line on the field sweep and this point projected vertically to the field versus time line gave the field at the ESR signal. A correction of .1% was added because the NMR probe was necessarily positioned out of the maximum field region. This and other factors put a limit of accuracy of about .2% on the absolute g-value but since the probe was in the same position for the whole

Table I Calculation of g value for a Sample Run

Temperature	Direction of Field Sweep	Measured g value	Averages	Overall Average
4.2 K	UP	1.76764	1.76751	1.76777
		747		
		742		
	DOWN	1.76809	1.76803	
		803		
		798		
1.7 K	UP	1.76774	1.76772	1.76785
		770		
	DOWN	1.76800	1.76798	
		796		

Measured Shift = .00008

Estimated Accuracy = .00010

experiment, it did not effect the g-shift measurement. The klystron frequency and NMR frequency measurements, made by an HP counter, were determined to an accuracy of at least 1 part in 10^6. Therefore, the main limit to precision was in the determination of the crossover point of the ESR signal on the baseline, which is dependent on the signal to noise ratio of the spectrometer.

A number of such trials were made at each temperature and the error in the average value thus obtained was approximated by giving the root mean square error. Table I shows the results of such an analysis where the error in the g-value was estimated at $\pm$ .0001.

An interesting feature of these data and other data collected was that there was a considerable difference between the g-values determined from sweeps with an increasing magnetic field and the g-value determined from sweeps with a decreasing magnetic field. This was not a time constant delay in the spectrometer since that would require a delay of about 3 seconds at the sweep speed used whereas the time constant as determined by the lock-in amplifier was set at 1 second. Similarly it was not due to the method of measuring the NMR frequency since that was set at a constant frequency and monitored every few seconds as the magnetic field approached the resonant condition. Thus, any

significant drift in the 4th or 5th figure would be easily detected. Also, the accuracy of this method can be approximated on an individual sweep basis by reference to Fig. 11. Here, it can be seen that the points come very close to the straight line drawn through them indicating an accuracy in terms of the time co-ordinate of about .5 seconds.

The g-value was taken as the mean between these two sweep dependent values and this mean showed no significant temperature variation in the 1.7°K to 4.2°K range.

Another effect observed in the data was the frequency drift in the cavity at 1.7°K. It was found that over the time period when the helium was being pumped the cavity frequency drifted from 9.2920 Gc to 9.2987 GHz, a change of .07%. The drift was assumed to be linear and when this correction was applied to the low temperature g-value calculations, values were obtained which were in very close agreement as can be seen in Table I. This drift was assumed to be due to the temperature dependence of various parameters of the cavity such as helium susceptability, and cavity length.

CHAPTER 5

CONCLUSIONS

The ESR signal of CdS(L) exhibited no measureable temperature variation between 1.7°K and 4.2°K. The line width of the signal at 9GHz was found to be $4.2 \pm .4$ gauss, but may have been subject to modulation broadening and further work is being done on this aspect. These results imply that at most the ESR technique can be used to set a better limit on the coefficient of the linear term, $Ck_{\perp}$, in the expression of $E(\bar{k})$, than the optical measurements of Hopfield. The present measurements indicate that C must be less than the 6×10^{-11} eVcm limit of Hopfield by a factor of $\sqrt{3} \approx 1.7$.

The temperature dependence observed at 35GHz remains unexplained and this will checked in greater detail when the 35GHz system in the laboratory is again operational. This shift could be accounted for by the normal resonant frequency change in cooling from 4.2°K to 1.7°K and the subsequent slow drifting as pumping was continued on the helium reservoir, if this drifting was not noticed.

The metal temperature controlled dewar system proved to be too noisy owing mainly to the fact that the modulation coils had to be mounted on the inside of the dewar because of skin depth losses combined with a

split cavity arrangement necessary to ensure thermal contact. Several suggestions are given for improving the system but it is concluded that a glass dewar system equiped with a reservoir for liquid helium to allow gas cooling would be a much more satisfactory arrangement.

APPENDIX I

CALIBRATION OF CARBON RESISTANCE THERMOMETER

Carbon is an intrinsic semiconductor and, as such, its electrical resistance increases sharply at low temperature. Thus, if it can be property calibrated, an ordinary carbon resistor can be used to obtain reasonably accurate low temperature readings.

Manufacturing peculiarities, particularly with regard to the bonding of leads, make most brands of carbon resistors unsuitable. Experiments have shown that an Allen Bradley, 33 ohm, $\frac{1}{2}$ watt is the most dependable. However, even with the Allen Bradley resistor, each thermal cycle can cause wide variation in the performance of the thermometer. This variation can be removed by the introduction of two arbitrary parameters Ro and To. Below in Fig.13 is shown the graph of $\log_e \frac{R}{Ro}$ against $\log_e \frac{T}{To}$ obtained by Clement, Dolecek, and Logan for these resistors.

Two reference points are required for the determination of Ro and To before temperature readings can be obtained. It was convenient in our apparatus to choose 77°K and 4.2°K, the boiling points of nitrogen and helium respectively. A computer program is given below which may be used to obtain Ro and To from

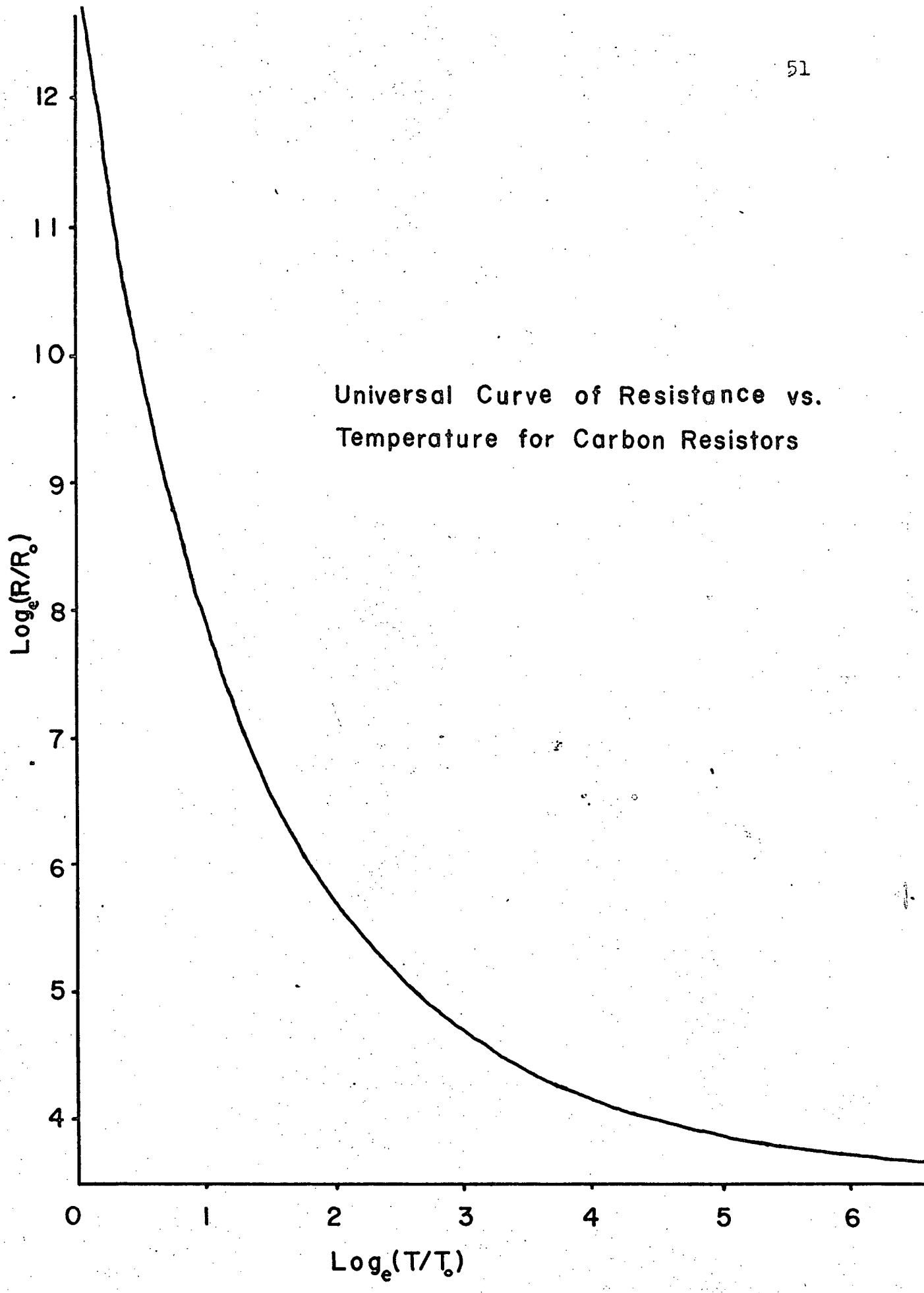
Universal Curve of Resistance vs.
Temperature for Carbon Resistors
12
11
10
9
8
7
6
5
4
0
1
2
3
4
5
6
$Log_e(R/R_o)$
$Log_e(T/T_o)$

Fig. 13

the reference point data and to print out temperatures for the subsequent resistances observed during the run.

```
1             DIMENSION X(52),Y(52)
2             READ 1,R1,T1,R2,T2,R0,T0
3           1 FORMAT(6F12.6)
4             DO 3 I=1,52,4
5             J=I+1
6             K=J+1
7             N=K+1
10          3 READ 4,X(I),Y(I),X(J),Y(J),X(K),Y(K),X(N),Y(N)
11          4 FORMAT(8F10.5)
12            COMMON X,Y
13            TOSUM=0.
14            ROSUM=0.
15            X1=ALOG(R1/R0)
16            Y1=ALOG(T1/T0)
17            X2=ALOG(R2/R0)
20            Y2=ALOG(T2/T0)
      C       T1C IS THE CALCULATED VALUE OF T1
21            DO 8 L=1,7
22            T1C=FINDT(X1)
23            TCOR=T1C-Y1
24            DO 5 I=1,52
25          5 Y(I)=Y(I)-TCOR
26            TOSUM=TOSUM+TCOR
27            R2C=FINDR(Y2)
30            RCOR=R2C-X2
31            ROSUM=ROSUM+RCOR
32            DO 6 I=1,52
33          6 X(I)=X(I)-RCOR
34            PRINT 7,TCOR,RCOR,TOSUM,ROSUM
35          7 FORMAT(20X,92H CORRECTION TO Y-VALS    CORRECTION TO X-VALS    T
             1TAL Y CORRECTION      TOTAL X CORRECTION//(20X,4F24.19))
36          8 CONTINUE
      C       THIS IS END OF FITTING PROCEDURE FOR TO AND RO
37            T0=T0/EXP(TOSUM)
40            R0=R0/EXP(ROSUM)
41            DO 9 I=1,52
42            X(I)=X(I)+ROSUM
43          9 Y(I)=Y(I)+TOSUM
      C       N IS THE NUMBER OF EXPERIMENTAL TEMPERATURES
44            READ 10,N
45         10 FORMAT(I5)
46            DO 11 I=1,N
47            READ 12,R
50         12 FORMAT(F20.10)
51            XE=ALOG(R/R0)
52            YE=FINDT(XE)
53            T=T0*EXP(YE)
```

```
54          11 PRINT 13, R,T,N
55          13 FORMAT(38X,11H RESISTANCE,20X,12H TEMPERATURE//(20X,2F32.25,I5,//
              1)
56             STOP
57             END
```

```
60             FUNCTION FINDR(V)
61             DIMENSION X(52),Y(52)
62             DIMENSION Z(4,6)
63             COMMON X,Y
64             DO 50 I=2,52
65          50 IF((Y(I)-V).LT.0.) GO TO 51
66          51 DO 70 K=1,4
67             L=I-3+K
70          70 Z(K,1)=Y(L)
71             DO 71 K=1,4
72             L=I-3+K
73          71 Z(K,2)=X(L)
74             DO 72 K=1,4
75             L=I-3+K
76          72 Z(K,6)=Y(L)-V
77             DO 52 J=3,5
100            M=J-2
101            DO 52 I=1,M
102         52 Z(I,J)=0.
103            DO 53 J=3,5
104            K=J-1
105            DO 53 I=K,4
106            L=I-1
107         53 Z(I,J)=(Z(L,K)*Z(I,6)-Z(I,K)*Z(L,6))/(Z(I,1)-Z(L,1))
110            FINDR=Z(4,5)
111            RETURN
112            END
```

```
113          FUNCTION FINDT(V)
114          DIMENSION X(52),Y(52)
115          DIMENSION Z(4,6)
116          COMMON X,Y
117          DO 40 I=2,52
120       40 IF((X(I)-V).GT.0.) GO TO 41
121       41 DO 60 K=1,4
122             L=I-3+K
123       60 Z(K,1)=X(L)
124             DO 61 K=1,4
125             L=I-3+K
126       61 Z(K,2)=Y(L)
127             DO 62 K=1,4
130             L=I-3+K
131       62 Z(K,6)=X(L)-V
132             DO 42 J=3,5
133             M=J-2
134             DO 42 I=1,M
135       42 Z(I,J)=0.
136             DO 43 J=3,5
137             K=J-1
140             DO 43 I=K,4
141             L=I-1
142       43 Z(I,J)=(Z(L,K)*Z(I,6)-Z(I,K)*Z(L,6))/(Z(I,1)-Z(L,1))
143             FINDT=Z(4,5)
144             RETURN
145             END
       $ENTRY
```

The first part of this program reads in the two reference points (R1, T1), (R2, T2) and the first approximation for R_o and T_o e.g. R_o=1, T_o=1. Fifty-two points are then read in from the graph of R/R_o against T/T_o and are put in a common pool with two FUNCTION subroutines. These two subroutines approximate R/R_o from a known value of T/T_o and T/T_o from a known value of R/R_o using an Aitken approximation procedure[10] and the

fifty-two values from the graph. Successive corrections are applied to R_o and T_o until they converge. Starting at about statement 9, the experimental resistances are read in and their corresponding temperatures are calculated using the final values of R_o and T_o and the FINDT subroutine. All pertinent data are then printed out under appropriate headings.

List of References

1. B.J. Slagsvold, 1966, Ph.D. Thesis (unpublished) and Ludwig, G.W. and Woodbury, H.H., 1963. Solid State Physics, Ed. by F. Seitz and D. Turnbull, Vol. 13 (Academic Press, Inc., New York) p. 223.

2. Birman, J.L., 1959. Phys. Rev. 114, 1490.

3. Hopfield, J.J., 1961. J. Appl. Phys. 32, Suppl. 2277.

4. Konopka, J., 1967. Phys. Lett. 26A, 29.

5. Kaplan, O. (private communication to J. Konopka).

6. Wilks, J., 1967. The Properties of Solid and Liquid Helium. (Clarendon Press, Oxford)

7. MacPherson, R., 1965. M.Sc. Thesis (unpublished).

8. Feher, G., 1957. Bell Systems Tech. J. 36, 449.

9. Poole, C.P. Jr., 1967. Electron Spin Resonance (John Wiley).

10. Fröberg, C.E., 1965. Introduction to Numerical Analysis (Addison-Wesley, Mass.) p. 150.